



Controlled Generation of Orbital Angular Momentum Beams With Coherent Beam Combining Digital Laser and Liquid-Crystal q-Plate

Corentin Lechevalier, Claude-Alban Ranély-Vergé-Dépré, Ihsan Fsaifes, Rezki Becheker, Gerben Boer, Jean-Christophe Chanteloup

► To cite this version:

Corentin Lechevalier, Claude-Alban Ranély-Vergé-Dépré, Ihsan Fsaifes, Rezki Becheker, Gerben Boer, et al.. Controlled Generation of Orbital Angular Momentum Beams With Coherent Beam Combining Digital Laser and Liquid-Crystal q-Plate. *IEEE Photonics Journal*, 2024, 16 (4), pp.1502305. 10.1109/JPHOT.2024.3421244 . hal-04740612

HAL Id: hal-04740612

<https://hal.science/hal-04740612v1>

Submitted on 12 Nov 2024

HAL is a multi-disciplinary open access archive for the deposit and dissemination of scientific research documents, whether they are published or not. The documents may come from teaching and research institutions in France or abroad, or from public or private research centers.

L'archive ouverte pluridisciplinaire **HAL**, est destinée au dépôt et à la diffusion de documents scientifiques de niveau recherche, publiés ou non, émanant des établissements d'enseignement et de recherche français ou étrangers, des laboratoires publics ou privés.

Controlled Generation of Orbital Angular Momentum Beams With Coherent Beam Combining Digital Laser and Liquid-Crystal q-Plate

Corentin Lechevalier^{ID}, Claude-Alban Ranély-Vergé-Dépré^{ID}, Ihsan Fsaifes^{ID}, Rezki Becheker^{ID}, Gerben Boer, and Jean-Christophe Chanteloup^{ID}

Abstract—We report on versatile orbital angular momentum beam generation through the association of a 61-channels coherent beam combining digital laser and a liquid-crystal q-plate. Particularly, high-order vortex beams that carry orbital angular momentum are generated with radial, azimuthal and/or circular polarization states. The q-plate is designed and manufactured to sustain high average power ensuring that the vortex spatial mode is preserved. The proposed system offers an extra degree of freedom for various applications requesting beam shaping with specific polarization state.

Index Terms—Coherent beam combining, phase control, OAM, q-plate, polarization control, structured light, high power laser.

I. INTRODUCTION

LIGHT degrees of freedom such as amplitude, phase, spin and orbital angular momentum (SAM/OAM) are key parameters for the generation of structured light. Vortex beams that carry orbital angular momentum are characterized by a helical wavefront carrying a phase singularity at the center. In the far-field, it results in a null central intensity surrounded by a donut-shaped distribution of light. These beams find widespread applications in high-field physics [1], among which: laser filaments range management, phase-structured beams, and optical communications. Traditional approaches to generate OAM beams rely generally on laser cavity tuning [2], phase plates [3], axicons [4], and spatial-light modulators (SLMs) [5]. The first ones allow high-output-power regime operation but lacks tunability. SLMs offer high tunability but are limited in output power by optical damage threshold.

Manuscript received 28 May 2024; accepted 26 June 2024. Date of publication 1 July 2024; date of current version 25 July 2024. This work was supported by European Innovation Council under Grant 101047223-NanoXCAN. (*Corresponding author: Corentin Lechevalier*)

Corentin Lechevalier, Ihsan Fsaifes, Rezki Becheker, and Jean-Christophe Chanteloup are with the LULI, CNRS, École Polytechnique, CEA, Sorbonne Université, Institut Polytechnique de Paris, 91120 Palaiseau, France (e-mail: corentin.lechevalier@polytechnique.edu; ihsan.fsaifes@polytechnique.edu; rezkibechecker@gmail.com; jean-christophe.chanteloup@polytechnique.fr).

Claude-Alban Ranély-Vergé-Dépré is with the Thales LAS France SAS, 78995 Elancourt, France, and also with LULI, CNRS, École Polytechnique, CEA, Sorbonne Université, Institut Polytechnique de Paris, 91120 Palaiseau, France (e-mail: claude-alban.raneley-verge-depre@polytechnique.edu).

Gerben Boer is with the Arcoptix SA, 2000 Neuchâtel, Switzerland (e-mail: boer@arcoptix.com).

Digital Object Identifier 10.1109/JPHOT.2024.3421244

In our previous work [6], we presented a versatile alternative approach, offering both practical high average powers and fast tunability, based on coherent beam combination of a large number of beamlines in the far-field. Mainly, we demonstrated the use of a 61 tiled channels coherent beam combination (CBC) femtosecond fiber amplifiers as a digital laser (DL) source to generate linearly polarized OAM beams. Each channel (beam) is considered as an individual pixel where amplitude and phase are addressed independently in real time. Adding the polarization control as a degree of freedom could offer more versatility towards a better control of the CBC far-field shaping, enabling new applications with specific polarization state and power distribution [7]. Recently, K. Ji et al. [8], demonstrated the generation of higher-order Poincaré sphere (HOPS) beams from a coherently combined six-core Yb-doped multicore fiber (MCF) amplifier, by using a spatial light modulator offering wavefront shaping and polarization control of the signals seeded into the individual cores of the MCF. E.V. Adamov et al., demonstrated recently the feasibility of controlling the polarization structure of synthesized beam (generated through coherent combination of six sub-beams) by changing the phase relations and polarization directions of the individual sub-beams [9].

In the case of our CBC digital laser, controlling the polarization of each beam within the fibered frontend is not suitable as all the 61 Ytterbium fiber amplifiers will impose the same linearly polarized amplification [10]. In this paper, we demonstrate far-field OAM beam engineering allowing global polarization control through the combined use of a tiled 61-channels CBC digital laser and a liquid-crystal q-plate designed and manufactured to guarantee high transmission and sustain high average power ensuring vortex spatial modes preservation.

In the following, quantities related to the digital laser are referred as *DL* while *q* indices are referring to the q-plate. Fast switching between spatial OAM modes is achieved by applying helical phase profiles $\rho_{\text{DL}}(k) = \sum_{k=1}^{61} e^{i\phi_k}$ to the 61 beams digital laser, where $\phi_k = l_{\text{DL}}\theta_k e[0, 2\pi]_k$, θ_k being the local (x, y) contribution of the azimuthal angle within the laser hexagonal composite pupil. Thus, the output vortex beam keeps a linear polarization carrying a topological charge l_{DL} defined as the number of turns the helical profile experiences for each electric field longitudinal periodic oscillation. A q-plate [11] is a phase plate with an azimuthal varying optical axis where the

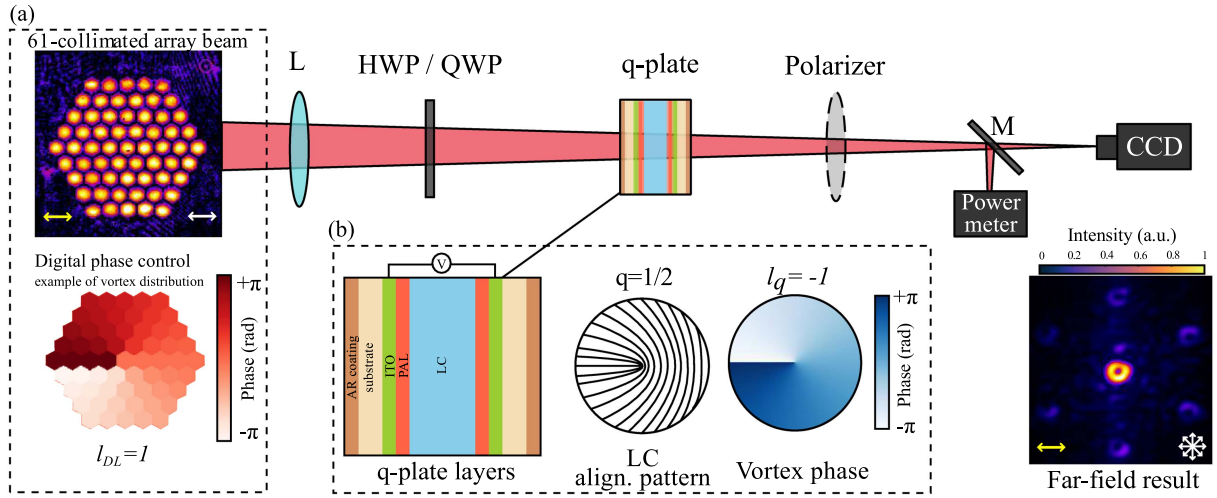


Fig. 1. A 61 channels digital laser with amplitude and phase profiles (a) is travelling through a q-plate carrying continuous vortex phase (b). HWP: Half-wave plate; QWP: Quarter-wave plate; L: Lens; M: Mirror. The yellow (white) arrows indicate the polarization orientation of the entering (existing) field.

tangent to the lines pattern displayed on Fig. 1(b) indicates the local direction of the optical axis. This retarder generates a $q\theta$ helical phase delay with θ the electrical field angular dependence expressed in polar coordinates $E(r, \theta) = E_0(r)e^{iq\theta}$.

The Jones matrix to be applied on this field at each point of the q-plate transverse plane is expressed according to linear polarization basis as follows [12]:

$$M_q = \begin{pmatrix} \cos(2q\theta) & \sin(2q\theta) \\ \sin(2q\theta) & -\cos(2q\theta) \end{pmatrix}. \quad (1)$$

The q-plate forms an OAM light from a beam with well-defined spin angular momentum (SAM). When illuminating the q-plate with uniform linear polarization, the beam is converted into radial $\begin{pmatrix} \cos\theta \\ \sin\theta \end{pmatrix}$ or azimuthal $\begin{pmatrix} \sin\theta \\ -\cos\theta \end{pmatrix}$ polarization depending of the q-plate principal axis. Passing through the q-plate, the beam will undergo a global helical phase $\rho_q = e^{i2q\theta}$ and earn a topological charge $l_q = 2q$. Thus, the photons of the beam have their SAM reversed and their OAM is increased by an amount of l_q . In this work, the q-plate features a fractional topological charge $q = 1/2$. It acts as a radial polarization converter generating vortices with charge $l_q = \pm 1$. The q-plate relies on a liquid crystal (LC) cell sandwiched between transparent electrodes that allows to efficiently tune the optical phase retardation of the q-plate [11]. Applying an electric field tilts the orientation of the LC nematic molecules along the optical axis. Consequently, the apparent index of refraction (tuned with applied voltage) varies between the ordinary and extraordinary indices. This leads to a phase shift between the polarization components parallel and perpendicular to the optical axis of $\phi(V) = \frac{2\pi}{\lambda} \Delta n(V) \cdot d$, where d is the thickness while $\Delta n = n_e(V) - n_o$ is the voltage dependant birefringence of the LC layer [11]. Associated with the CBC digital laser, this q-plate allows to generate high average power coherently combined OAM beam with polarization control.

The polarization state of the 61 channels composite near-field (Fig. 1(a)) is defined by the polarization maintaining fiber

amplifiers which provide a linearly polarized amplification. In order to obtain a radially or azimuthally polarized beams, a q-plate needs to be added in the beam path. We can interpret the action of the q-plate on the incoming polarized beam by considering the Jones formalism. As already stated, the linear polarizations of the 61 input beams are all aligned along the same axis giving a global horizontally polarized mode $\begin{pmatrix} 1 \\ 0 \end{pmatrix}$. This mode is then sent to the q-plate (1) to obtain an output radially polarized beam [12]:

$$\begin{aligned} M_{rad} &= \begin{pmatrix} \cos(2q\theta) & \sin(2q\theta) \\ \sin(2q\theta) & -\cos(2q\theta) \end{pmatrix} \cdot \begin{pmatrix} 1 \\ 0 \end{pmatrix} \cdot e^{i\phi_k} \\ &= \begin{pmatrix} \cos(2q\theta) \\ \sin(2q\theta) \end{pmatrix} \cdot e^{il_{DL}\theta}. \end{aligned} \quad (2)$$

When a beam is carrying a right circular polarization $\frac{1}{\sqrt{2}} \begin{pmatrix} 1 \\ i \end{pmatrix}$, he gets transformed into left circular polarization $\frac{1}{\sqrt{2}} \begin{pmatrix} 1 \\ -i \end{pmatrix}$ at the output of the q-plate. The resulting Jones matrix for a circular input polarization leads to a total topological charge $l = l_{DL} + l_q$ as follows:

$$\begin{aligned} M_{circ} &= \begin{pmatrix} \cos(2q\theta) & \sin(2q\theta) \\ \sin(2q\theta) & -\cos(2q\theta) \end{pmatrix} \cdot \frac{1}{\sqrt{2}} \begin{pmatrix} 1 \\ i \end{pmatrix} \cdot e^{i\phi_k} \\ &= \frac{1}{\sqrt{2}} \begin{pmatrix} 1 \\ -i \end{pmatrix} \cdot e^{i(l_{DL}+l_q)\theta} \\ &= \frac{1}{\sqrt{2}} \begin{pmatrix} 1 \\ -i \end{pmatrix} \cdot e^{il\theta}. \end{aligned} \quad (3)$$

II. EXPERIMENTAL RESULTS

The digital laser architecture relies on a tiled-aperture configuration, where 61 polarized Yb-fiber amplifiers are placed side-by-side as close to each other as possible in a planar hexagonal array arrangement (Fig. 1(a)). The phase of each

individual beam is controlled in real time through the combined use of variable optical delay lines and piezo-mechanical fiber stretchers [10]. Conventionally, an in-phase pattern (flat phase) in which all 61-beam phases are identical $\phi_k = 0, \forall k$ is used. The phase stabilization (at ~ 1 kHz) is performed using an interferometric measurement method with active phase control. The CBC is achieved when focusing the composite pupil with a single lens (L). As the composite near-field is made of Gaussian output beams, its intensity is periodically modulated, and gives rise, in the far-field, to sidelobes surrounding the CBC main lobe [6]. When applying a helicoidal phase $e^{il_{DL}}$ distribution to the 61-channels, an OAM beam (donut shape) characterized by its topological charge l_{DL} is generated in the far-field. For this study, all the fiber channels deliver the same output optical average power.

The q-plate, designed and manufactured with an active area of 20 mm and withstanding a \sim kW average power, is inserted in the path of the pixelated laser after the lens (Fig. 1(b)). A half-waveplate (HWP) is inserted to properly control the orientation of the linearly polarized 61 beams with respect to the q-plate principal axis. A polarizer is placed before the CCD camera to analyze the polarization state.

At high average power laser operation, heat load across the q-plate can cause significant phase shift variations. This is due to the relatively important temperature dependency of the LC birefringence (0.5 %/K) [13]. These phase distortions will deform the amplitude profile and cause efficiency losses. To reduce heat absorption, a q-plate that minimizes light absorption has been developed. As shown in the inset (b) of Fig. 1, when the light propagates through the q-plate, it first passes through an anti-reflection coating (AR), followed by a 3 mm thick transparent substrate, a thin transparent (Indium-Tin-Oxide, ITO) electrode, a (\sim 200 nm) photo-alignment layer (PAL) which contains planar anchor to guide the LC in a layout related to the topological charge $q = 1/2$ [11]; see the alignment pattern of the LC on Fig. 1(b). Finally, the liquid crystal (LC) layer is 20 μm thick. Light absorption is mainly caused by the substrates and electrodes. The absorption caused by the LC is not significant [11]. In order to transfer efficiently the heat towards the water-cooled LC cell housing, the substrate must also carry a high thermal conductivity. Furthermore, to avoid additional phase distortion, it should also have a low birefringence. To fulfil all the aforementioned constraints, we choose to rely on AR coated sapphire substrates and a 100 nm thick ITO transparent electrode. Indeed, sapphire exhibits a low absorption (100 ppm/cm at 1 μm), a very good thermal conductivity (25 W/m/K) and a low birefringence (0.01 at 1 μm). Ultimately, the largest absorption contribution is due to ITO layer (absorption coefficient is 500 cm^{-1} at 1 μm leading to 2–3% absorption). The 93% transmitted light hits the mirror M where a 0.1% fraction is transmitted to a CCD camera placed at the focal plane for spatial diagnostics, while the reflected part is directed towards a power-meter.

As a first experiment, the digital laser is operated with a flat phase $\phi_k = 0 \forall k$ (i.e., $l_{DL} = 0$). Then, only the vortex phase from the q-plate is contributing to the resulting phase with $l_q = -1$. On Fig. 2, the polarization states of the beam are analyzed in the near-field (top) and far-field (bottom). Fig. 2(a)

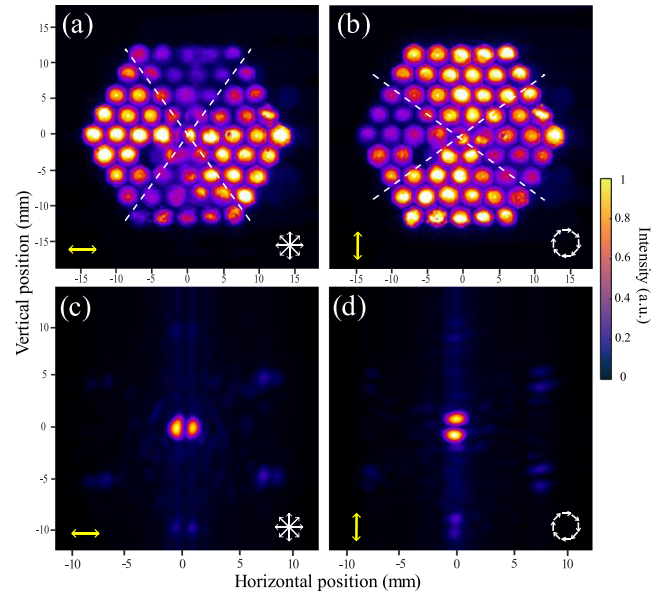


Fig. 2. Near-fields (a), (b) and far-fields (c), (d) intensity distributions observed after the linear polarizer. Polarization state of the beam entering (exiting) the q-plate is depicted with yellow (white) arrows.

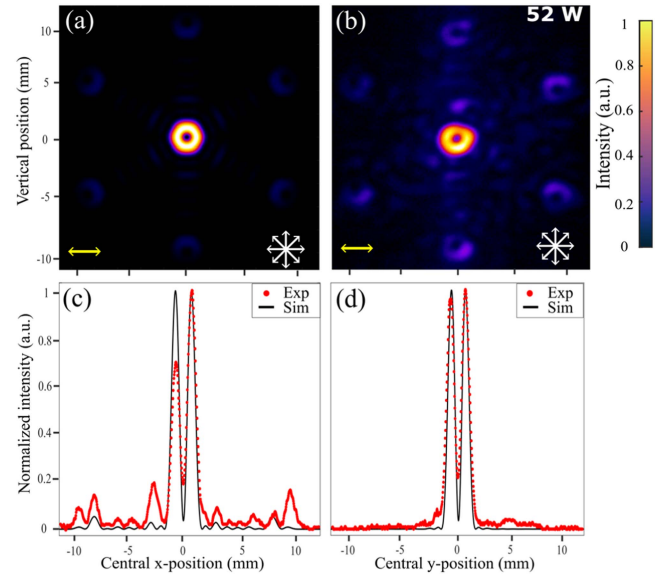


Fig. 3. Simulated (a) and experimental (b) radially polarized (white arrow) ring pattern obtained with linear incident polarization (yellow arrow) on the q-plate. Panels (c) and (d) are, respectively, vertical and horizontal intensity distribution across the beam.

and (b) displays the near-field intensity distributions obtained when using a HWP and the polarizer. As the polarization of the incoming laser is linear (yellow arrow), the polarization state of the pattern exiting the q-plate (white arrow) is either radial (Fig. 2(a) and (c)) or azimuthal (Fig. 2(b) and (d)). For instance, when the HWP is oriented horizontally (Fig. 2(a)) the 61 sub-pupils near-field exhibits a horizontal hourglass-shaped pattern with bright and dark sectors (bordered by the white dashed lines). In the same way, Fig. 2(c) and (d) show the far-field

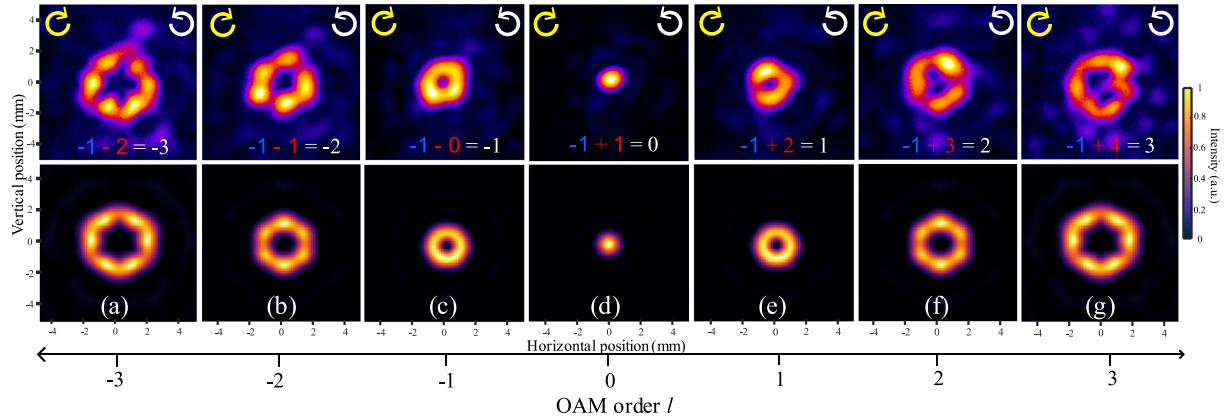


Fig. 4. Far-fields OAM generated when associating q-plate (blue numbers) with helical phase applied on the digital laser (red numbers). Top (bottom) experimental (simulated) far-fields for different azimuthal indices from $l = -3$ (a) to $l = +3$ (g).

states. For each orientation, a dumbbell shape (double lobes) is obtained and oriented in the same way as the near-field. This behavior is also observed on the six sides lobes surrounding the central one.

Let us now consider the generated ring shape by removing the polarizer in front of the CCD camera. Fig. 3(a) and (b) show typical far-field intensity distribution for a defined HWP reference angle (horizontal yellow arrow) giving a radially polarized beam (white arrow). The central beam reveals a uniform ring shape surrounded by six weaker side beams. A good agreement is obtained between experimental and simulation results, when looking on the vertical and horizontal beam intensity profiles (Fig. 3(c) and (d)).

From now on, we remove the polarizer and replace the HWP by a quarter-waveplate (QWP) to generate a circularly polarized beam.

At the output of the QWP, a clockwise circularly polarized beam is obtained and converted to counterclockwise polarized beam after passing through the q-plate. An interesting result is then obtained when combining the topological charge from the phase control (l_{DL}) with the one from the q-plate (l_q). The corresponding recorded experimental far-fields images are displayed in the top images of Fig. 4, while being compared to simulations (bottom images). When using the q-plate together with a flat phase $\phi_k = 0 \forall k$ (i.e., $l_{DL} = 0$, red numbering) on the 61-channels laser, a circularly polarized beam (with a fixed topological charge $l_q = -1$, blue numbering) is obtained, as shown on Fig. 4(c). Applying a digital helical phase ϕ_k onto the 61 channels digital laser, one achieves first to compensate exactly the vortex phase from the q-plate with an opposite phase profile. Consequently, the total topological charge considers both the phase contribution from the digital laser and the q-plate, leading to $l = l_{DL} + l_q = 0$ ($l_{DL}(l_q)$ are red (blue) number on Fig. 4); thus, the total phase profile of the beam is flat and we get the fundamental Gaussian mode, as shown on Fig. 4(d).

The digital laser offers the possibility to go further by applying higher orders phase profiles with l_{DL} taking values up to 4 in this work. When the q-plate is combined with the helical phase applied to the digital phase control at different orders, higher

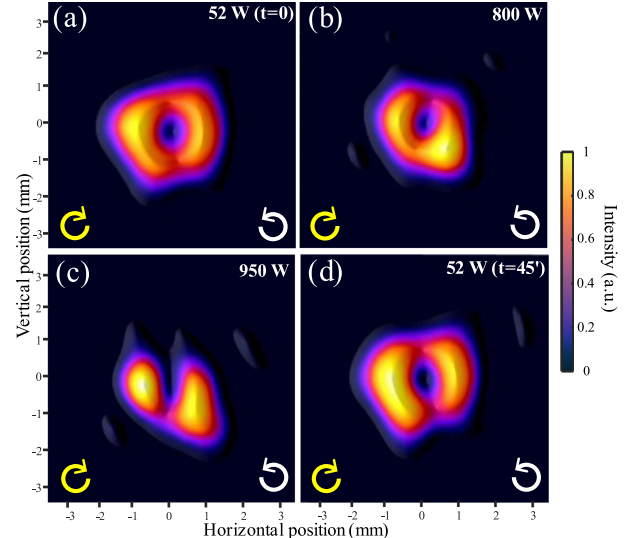


Fig. 5. Power ramp-up of an OAM ($l = 1$). The central beam low power (a) (52 W at $t = 0$) is progressively increased to 800 W (b) and 950 W (c), then reduced back to 52 W after 45 min of operation (d).

order polarized OAM beams are then generated (white numbers on Fig. 4). Higher order OAM beams with total topological charges of $l = -3$ to $+3$ are depicted in Fig. 4(a)–(g) while applying a digital helical phase order with l_{DL} varying between -2 and +4 (red). Each amplitude profile of the OAM mode depicted on Fig. 4 is individually normalized. It should be noted that for both simulation and experimental results (Fig. 4(a)–(g) top and bottom), ring intensity profiles are not perfectly uniform. To improve the smoothness of the donut shape of high orders OAM ($l > 3$), one possibility is to add extra rings of fiber amplifiers (i.e., “pixels”) around the actual digital laser array, increasing thereby the digital laser resolution. The second possibility, presently under investigation, is to assess the capability of iterative computing approaches like deep learning and genetic algorithms (GAs) to homogenize the far field radial intensity distribution of the OAM beams generated by the CBC femtosecond digital laser [14].

Finally, we evaluate the ability for the q-plate to hold high average power. Fig. 5 displays far-field central beam for several average power values. The circular polarized donut beam keeps its shape upon a power of 800 W. When the laser reaches average power up to 950 W some degradations start to be observed (Fig. 5(c)). This is likely to be related to the LC housing water-cooling system limitation. To confirm this statement, we operated the q-plate several times to generate the donut pattern both at low and high average powers. At low power, we retrieve the same initial intensity distribution (Fig. 5(d)), dismissing any degradation of the q-plate due to thermal load.

III. CONCLUSION

In summary, we have experimentally demonstrated OAM beams featuring different polarization states when associating the 61-channels coherent beam combining digital laser with a liquid-crystal q-plate. The CBC digital laser allows scalability and digital phase control, while the q-plate generates structured light beam with polarization control. The q-plate is tailored to the laser array size, designed and manufactured to guarantee high transmission and sustain high average power ensuring vortex spatial modes preservation. When only the laser phase control is operated (i.e., without the q-plate), the polarization state of the donut created in the far-field remains linear. In other words, the digital laser without q-plate is purely OAM acting and the SAM stays unchanged. When the q-plate is placed downstream the digital laser, the beam can get new polarization states, like radial, azimuthal or circular states. The presented results illustrate the possibility to associate a dynamic CBC digital laser with a continuous q-plate to control separately the OAM and SAM component of the generated beam [15]. The proposed system offers an extra degree of freedom for various applications requesting beam shaping with specific polarization state, among which, particle acceleration [16], optical trapping [17], and laser material processing [18]. Finlay, to generate high order and/or complex structured light beams with amplitude, phase and polarization control, the CBC digital laser resolution (numbers of pixels or beams) and/or the q-plate topological charge (l_q) need to be increased. Several q-plates could as well be used in cascade [19] to generate higher vortex beams with polarization diversity.

REFERENCES

- [1] M. Zürch, C. Kern, P. Hansinger, A. Dreischuh, and C. Spielmann, "Strong-field physics with singular light beams," *Nature Phys.*, vol. 8, no. 10, pp. 743–746, Oct. 2012, doi: [10.1038/nphys2397](https://doi.org/10.1038/nphys2397).
- [2] D. Naidoo et al., "Controlled generation of higher-order Poincaré sphere beams from a laser," *Nature Photon.*, vol. 10, pp. 327–332, 2016.
- [3] M. W. Beijersbergen, R. P. C. Coerwinkel, and M. Kristensen, "Helical-wavefront laser beams produced with a spiral phaseplate," *Opt. Commun.*, vol. 112, no. 5/6, pp. 321–327, 1994.
- [4] N. Ochiai, J. Shou, and Y. Ozeki, "Axiicon-based beam shaping for low-loss nonlinear microscopic optics," *J. Opt. Soc. Amer. B*, vol. 36, pp. 1342–1347, 2019.
- [5] S. Ngcobo, I. Litvin, L. Burger, and A. Forbes, "A digital laser for on-demand laser modes," *Nature Commun.*, vol. 4, 2013, Art. no. 2289.
- [6] M. Veinhard et al., "Orbital angular momentum beams generation from 61 channels coherent beam combining femtosecond digital laser," *Opt. Lett.*, vol. 46, pp. 25–28, 2021.
- [7] I. Fsaifes, C.-A. Ranély-Vergé-Dépré, M. Veinhard, S. Bellanger, and J.-C. Chanteloup, "Far field energy distribution control using a coherent beam combining femtosecond digital laser," *Opt. Exp.*, vol. 31, pp. 8217–8225, 2023.
- [8] K. Ji et al., "Controlled generation of picosecond-pulsed higher-order Poincaré sphere beams from an ytterbium-doped multicore fiber amplifier," *Photon. Res.*, vol. 11, pp. 181–188, 2023.
- [9] E. V. Adamov, E. A. Bogach, V. V. Dudorov, V. V. Kolosov, and M. E. Levitskii, "Controlling the polarization structure of vector beams synthesized by a fiber laser array," *Opt. Commun.*, vol. 559, May 2024, Art. no. 130399, doi: [10.1016/j.optcom.2024.130399](https://doi.org/10.1016/j.optcom.2024.130399).
- [10] I. Fsaifes et al., "Coherent beam combining of 61 femtosecond fiber amplifiers," *Opt. Exp.*, vol. 28, pp. 20152–20161, 2020.
- [11] A. Rubano, F. Cardano, B. Piccirillo, and L. Marrucci, "Q-plate technology: A progress review," *J. Opt. Soc. Amer. B*, vol. 36, pp. D70–D87, 2019.
- [12] L. Marrucci, C. Manzo, and D. Paparo, "Optical spin-to-orbital angular momentum conversion in inhomogeneous anisotropic media," *Phys. Rev. Lett.*, vol. 96, 2006, Art. no. 163905.
- [13] Z. Alipanah, M. S. Zakerhamidi, and A. Ranjkesh, "Temperature-dependent optical properties of some mixtures nematic liquid crystal," *Sci. Rep.*, vol. 12, 2022, Art. no. 12676.
- [14] C.-A. Ranély-Vergé-Dépré, R. Becheker, I. Fsaifes, M. Burger, I. Jovanovic, and J.-C. Chanteloup, "Experimental optimization of orbital angular momentum beams generated by coherent beam combining digital laser," in *Proc. Adv. Solid State Lasers*, 2023, Paper JTU5A, doi: [10.1364/ASSL.2023.JTu5A.4](https://doi.org/10.1364/ASSL.2023.JTu5A.4).
- [15] Z. Liu et al., "Generation of arbitrary vector vortex beams on hybrid-order Poincaré sphere," *Photon. Res.*, vol. 5, pp. 15–21, 2017.
- [16] V. Marceau, A. April, and M. Piché, "Electron acceleration driven by ultrashort and nonparaxial radially polarized laser pulses," *Opt. Lett.*, vol. 37, pp. 2442–2444, 2012.
- [17] X. Wang, Y. Zhang, Y. Dai, C. Min, and X. Yuan, "Enhancing plasmonic trapping with a perfect radially polarized beam," *Photon. Res.*, vol. 6, pp. 847–852, 2018.
- [18] K. Masuda et al., "Nanoscale chiral surface relief of azo-polymers with nearfield OAM light," *Opt. Exp.*, vol. 26, pp. 22197–22207, 2018.
- [19] Y.-W. Huang et al., "Versatile total angular momentum generation using cascaded J-plates," *Opt. Exp.*, vol. 27, pp. 7469–7484, 2019.